Appl Phys A (2011) 104:357–364
DOI 10.1007/s00339-010-6149-3

Applied Physics A
Materials Science & Processing

Irradiation of amorphous $Ta_{42}Si_{13}N_{45}$ film with a femtosecond laser pulse

V. Romano · M. Meier · N.D. Theodore · D.K. Marble · M.-A. Nicolet

Received: 10 September 2010 / Accepted: 6 October 2010 / Published online: 14 December 2010
© Springer-Verlag 2010

Abstract Films of 260 nm thickness, with atomic composition $Ta_{42}Si_{13}N_{45}$, on 4″ silicon wafers, have been irradiated in air with single laser pulses of 200 femtoseconds duration and 800 nm wave length. As sputter-deposited, the films are structurally amorphous. A laterally truncated Gaussian beam with a near-uniform fluence of $\sim$0.6 J/cm^2 incident normally on such a film ablates 23 nm of the film. Cross-sectional transmission electron micrographs show that the surface of the remaining film is smooth and flat on a long-range scale, but contains densely distributed sharp nanoprotrusions that sometimes surpass the height of the original surface. Dark field micrographs of the remaining material show no nanograins. Neither does glancing angle X-ray diffraction with a beam illuminating many diffraction spots. By all evidence, the remaining film remains amorphous after the pulsed femtosecond irradiation.

The same single pulse, but with an enhanced and slightly peaked fluence profile, creates a spot with flat peripheral terraces whose lateral extents shrink with depth, as scanning electron and atomic force micrographs revealed. Comparison of the various figures suggests that the sharp nanoprotrusions result from an ejection of material by brittle fraction and spallation, not from ablation by direct beam–solid interaction. Conditions under which spallation should dominate over ablation are discussed.

V. Romano (✉) · M. Meier
Institute of Applied Physics, University of Bern, Bern, Switzerland
e-mail: valerio.romano@iap.unibe.ch

V. Romano
Bern University of Applied Sciences, Burgdorf BE, Bern, Switzerland

N.D. Theodore
Freescale Semiconductor Inc., Tempe, AZ, USA

D.K. Marble
Tarleton State University, Stephenville, TX, USA

M.-A. Nicolet
California Institute of Technology, Pasadena, CA, USA
e-mail: man@caltech.edu

1 Introduction and aim of the study

How laser beams interact with solids has been investigated very extensively in the past [1, 2]. New questions are now accessible as femtosecond pulses of adequate intensity have become available. One focus has been to determine the fluence thresholds for the transformation of a target, motivated principally by the hope of applications in industrial processing. Such investigations typically start with single crystalline materials whose changes are monitored with various analytical tools as a function of the fluence of the pulse or the number of pulses applied sequentially to the same spot, as well as in evolution of time.

The present experimental study proceeds differently. The initial sample is a thin film of a structurally amorphous material. The aim is to ascertain how little the film is altered upon ablation by a very brief laser pulse. Two questions are addressed specifically:

- Is it possible to ablate fractional thicknesses of an amorphous thin film with laser irradiation?
- Is it possible to accomplish that without inducing crystallization in the remaining part of the film?

2 Experimental procedures

The film we have studied consists of tantalum, silicon, and nitrogen. It is one of a class of materials (mictamict ma-

terials [3]) that may be conceptually viewed as composed of two immiscible binary compounds with one common element, in the present case TaN and Si_3N_4. Typical for these binary compounds is their mutual immiscibility based on dissimilar crystalline structures, different atomic sizes of the constituting elements, and often dissimilar character of bonding. One of the useful attributes of mictamict materials is that their electrical resistivity is adjustable over wide ranges by changes in composition. Another is their near-amorphous or entirely amorphous structure under analysis by X-ray diffraction or even high-resolution transmission electron microscopy. Furthermore, mictamict materials have the uncommon ability to withstand thermal annealing under elevated temperatures without crystallizing. Together, these properties offer new capabilities as thin-film components in electronic systems for extreme conditions.

We have chosen films of Ta–Si–N because this material resists crystallization under one of the highest thermal annealing cycles recorded for such alloys (over 1/2 h at 800°C in vacuum [4]). For their synthesis, the films were reactively sputter-deposited on bare 4″ n-type ⟨100⟩ silicon wafers. The as-deposited films were analyzed by 2.0 or 1.5 MeV He^4 backscattering spectrometry for atomic composition and by planar transmission electron diffraction for structure. Cross-sectional transmission electron micrographs before and after irradiation were taken to determine how much material had been removed, what the surface morphology of the remaining film looked like, and if crystalline grains could be detected there. The cross-sectional samples were prepared by the focused ion beam lift-off technique.

The atomic composition of the film is $Ta_{42}Si_{13}N_{45}$ with a few at.% argon mixed in. The film thickness is about 260 nm $\leq \pm 5$ nm. The uncertainty most likely originates from where a particular sample of the film came from on the 4″ silicon wafer. Diffuse rings from conventional planar transmission electron diffraction patterns confirm that the film is amorphous as deposited.

For the ablations we have selected a femtosecond pulsed laser to favor ablation while limiting the odds of altering the bulk of the film. The setup consisted of a mode locked Ti:sapphire seed oscillator delivering pulses of 100 fs duration at 800 nm wavelength and 85 MHz repetition rate. After being stretched, amplified, and compressed again, a pulse's duration was about 200 fs with a maximum energy of 1 mJ. A shutter and a target scanner enabled us to perform ablations in air with single pulses of an approximately rectangular area of 80 × 70 μm^2. Unless stated otherwise, the lateral beam intensity was kept as uniform as possible by truncating the Gaussian beam to its central maximum with a rectangular aperture.

3 Results

Figure 1(a) shows a scanning electron micrograph of a 1.0×0.81 mm^2 area of a film after ablation with single femtosecond pulses of about 0.6 J/cm^2 fluence and a synchronized displacement of the film. Figure 1(b) indicates that the beam intensity varies somewhat over its area and that the image of the rectangular beam aperture is distorted by the optics of the system. Cross-sectional transmission electron micrographs offer a detailed view of the surface morphology after material removal by the laser pulse. One sees in Fig. 2(a) that the removed layer is about 23 nm thick and laterally uniform. Two notable features appear in the micrograph. Firstly, the edge of the ablation spot is marked with a rim that consists of a short segment of an uplifted layer whose thickness equals that of the removed material

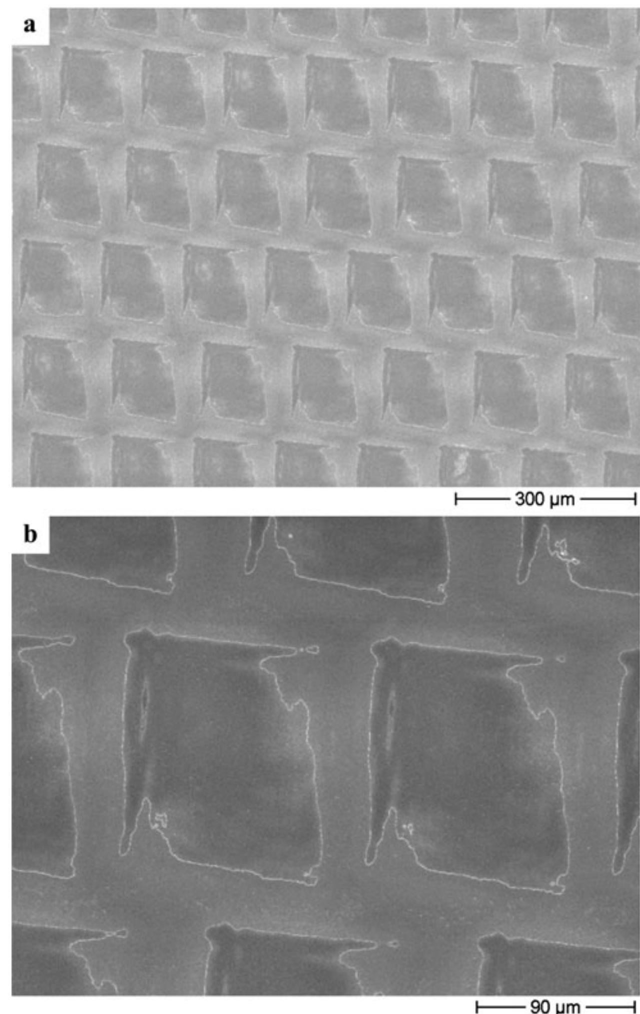

Fig. 1 Scanning electron micrograph of a wide view (*top*) and an enlarged view (*bottom*) of ablation spots produced with a 200 fs pulse of 800 nm wave length in an amorphous $Ta_{42}Si_{13}N_{45}$ film on a silicon substrate. The average fluence was 0.6 J/cm^2. The elongated shadow towards the left side of the spot is more deeply ablated than the remainder of the spot because of a local nonuniformity of the fluence

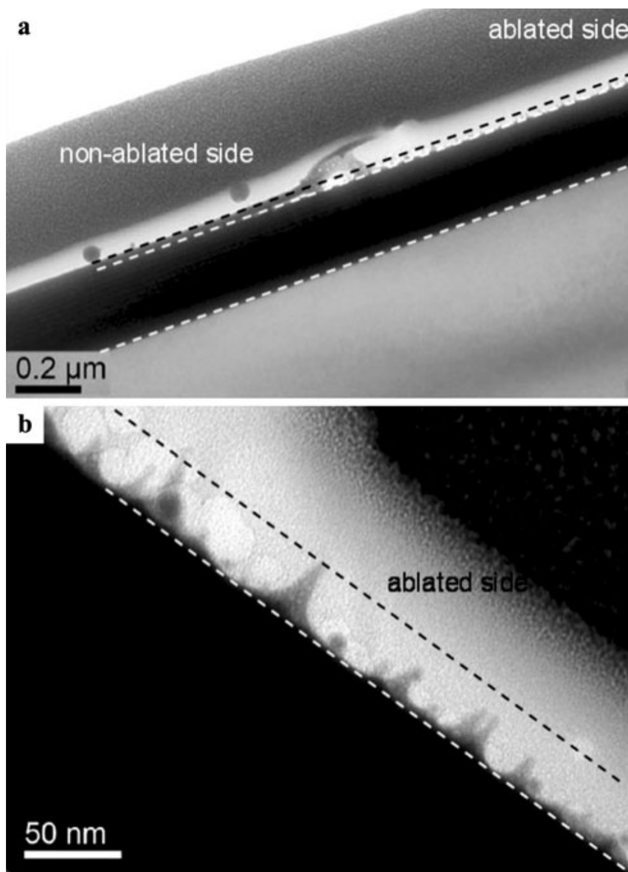

Fig. 2 Bright field cross-sectional transmission electron micrograph of an ablation spot of the sample of Fig. 1. (**a**) View of the border between irradiated (*right*) side and non-irradiated (*left*) side of the spot. (**b**) Magnified view of the irradiated side

(Fig. 2(a)). This feature or one equivalent to it is seen in all cross-sectional micrographs that depict the edge of an irradiated area (e.g., Figs. 3(a), 4(a)). This attribute is thus generic of the material removal process. The feature extends around the whole ablation spot. Indeed, one sees a bright line running along the periphery of each irradiated spot in the scanning electron image of Fig. 1(b). Sharp protrusions are known to enhance the emission of secondary electrons. Secondly, the surface of the film after irradiation is smooth on a scale long compared to the removed thickness but contains numerous sharp pyramid-like nanoprotrusions whose heights are on the scale of the removed thickness. Their heights sometimes even surpass that of the original surface before ablation (Fig. 2(b)). Scanning electron microscopy with adequate lateral resolution has established that these nanoprotrusions are isolated objects. They are randomly distributed over the whole ablated area and are not restricted to the proximity of the ablation edge as depicted in Figs. 2(a) or 4(a).

Figures 3(a), (b), (c) display cross-sectional micrographs of a film that was ablated with a pulse of the same duration of 200 fs but at an enhanced fluence (1.5 J/cm^2).

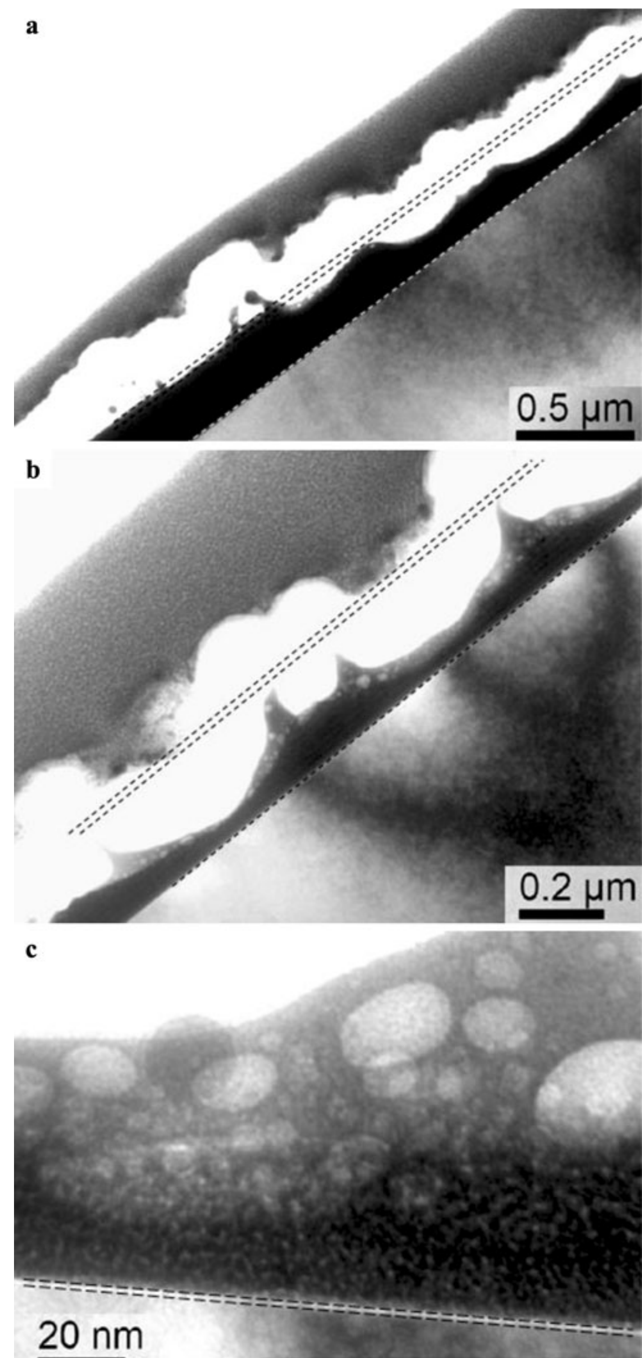

Fig. 3 Bright field cross-sectional transmission electron micrograph of an ablation spot produced with a 200 fs pulse of 800 nm wave length in an amorphous $Ta_{42}Si_{13}N_{45}$ film on a silicon substrate. The average fluence was 1.5 J/cm^2. (**a**) View of the border between irradiated (*right*) side and non-irradiated (*left*) side of the spot. (**b**) Magnified view of an irradiated part of (**a**). (**c**) High magnification of a part of (b)

About 2/3 of the initial film thickness is removed in this case. The surface that remains after ablation is again topographically structured (Fig. 3(b)) but on a roughly ten times coarser lateral scale than at the lower fluence of Fig. 2. Disc-like regions of enhanced electron transparency are clearly

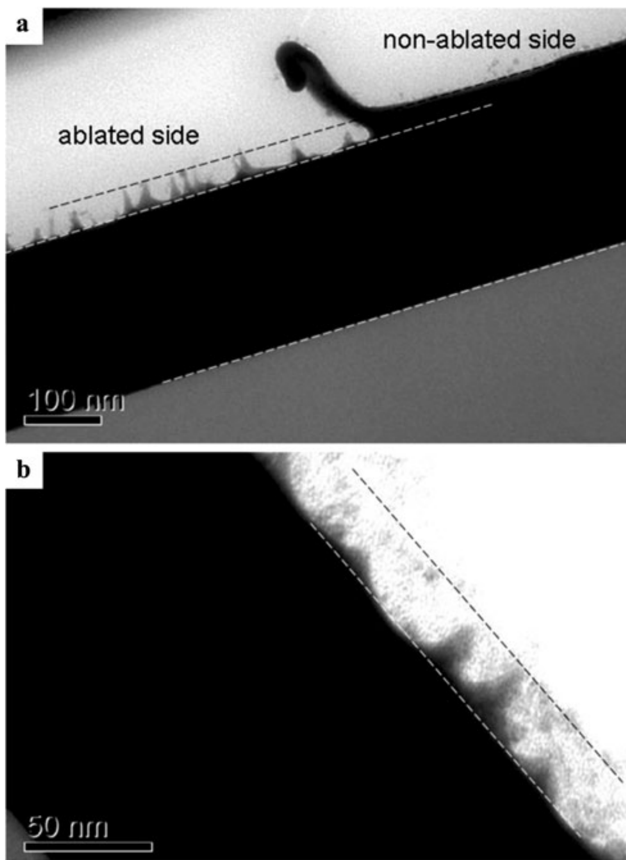

Fig. 4 Bright field cross-sectional transmission electron micrograph of an ablation spot produced with a 200 fs pulse of 800 nm wave length in an amorphous $Ta_{58}Si_{24}O_{18}$ film on a silicon substrate. The average fluence was 0.6 J/cm^2. (**a**) View of the border between irradiated (*left*) side and non-irradiated (*right*) side of the spot. (**b**) Magnified view of the irradiated side of (a)

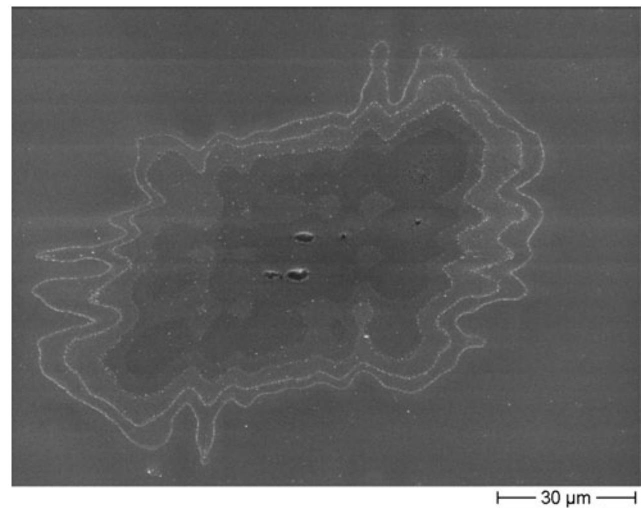

Fig. 5 Scanning electron micrograph of an ablation spot on a $Ta_{58}Si_{24}O_{18}$ film formed with a single 200 fs pulse of 800 nm wave length. The beam intensity decreases monotonically but not symmetrically from the center outwards. The picture measures 137 × 104 µm^2. Similar results are obtained on $Ta_{42}Si_{13}N_{45}$ films

seen in Fig. 3(b) and especially so at the high magnification of Fig. 3(c). These regions of enhanced transparency are present in large numbers. Their shapes strongly suggest that these regions are volumes of near-spherical shape and possibly filled with gaseous nitrogen. Their size increases with proximity to the surface while their number rises away from the surface. These features exist also after ablation at the low fluence of Fig. 2(a) (see the short segment of the uplifted layer at the edge of the ablation region); their size is substantially less, however.

Dark-field TEM micrographs were attempted from a peak such as those seen in Fig. 3(b) to look for possible crystalline grains. Good images were difficult to obtain in the presence of the heavy tantalum. It can be stated nonetheless that if there are crystalline grains, they are at most nm in size or less and few in numbers. The film material remaining after ablation is basically still amorphous. X-ray diffraction analysis of an irradiated $Ta_{42}Si_{13}N_{45}$ film with a glancing incident angle of the beam to enhance the sensitivity and which illuminated a total area with many ablation spots did not display any sharp lines that could be attributed to crystalline grains. Although still amorphous, the near-surface layer of the remaining film may possibly have a composition that is leaner in nitrogen than the bulk of the film.

To check whether nitrogen is associated with the development of the near-spherical features in Figs. 2 and 3, we tested a 254 nm-thick film that was deposited on bare silicon without intentionally adding nitrogen to the sputtering gas. MeV He^4 backscattering spectrometry yielded an atomic composition for this film of $Ta_{58}Si_{24}O_{18}$ (also a mictamict material). Some oxygen was evidently present inadvertently in the deposition system during the sputter-deposition of the film. Analysis by planar transmission electron diffraction produced diffuse rings which confirm that this film is also structurally amorphous as deposited. Irradiation with the laser at the same average fluence of ∼0.6 J/cm^2 used for the sample of Figs. 2(a), (b) removed 27 nm of material (Fig. 4(a)) which is close to the 23 nm obtained for the $Ta_{42}Si_{13}N_{45}$ film. No sphere-like features like those depicted in Figs. 2 and 3 are seen (Fig. 4(b)). By this evidence, nitrogen is, in fact, associated with the enhanced electron-transparency features in Figs. 2 and 3 that are hence likely filled with gaseous nitrogen. Nanoprotrusions exist in the nitrogen-free material as well. It thus follows that the mechanisms that lead to the formation of the nanoprotrusions and to the voids are distinct.

In contrast to the situation of Figs. 1 to 4 where the laser beam had a fluence that was laterally almost constant, the ablation spot shown in Fig. 5 was generated with a single laser pulse whose fluence was laterally not uniform but was rising monotonically towards a gentle maximum at the cen-

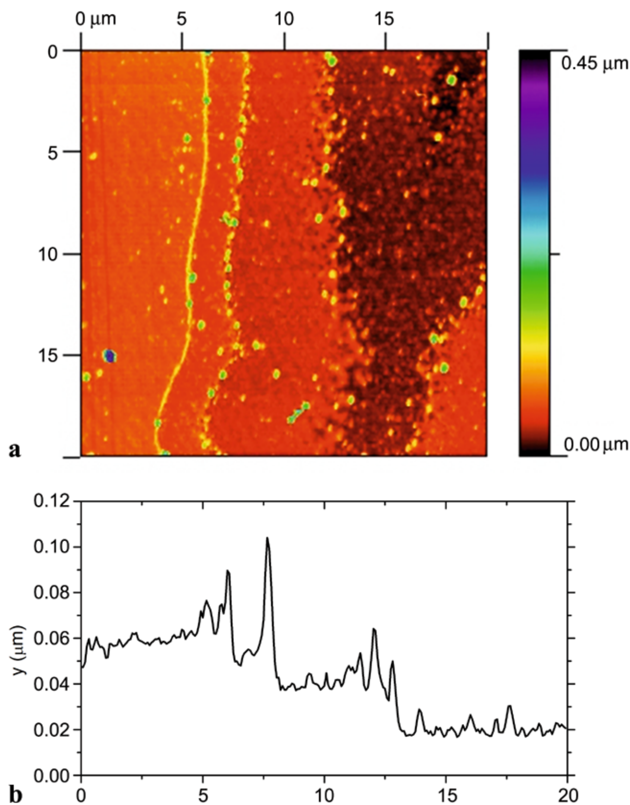

Fig. 6 (**a**) Atomic force micrograph of a selected area of the ablation spot depicted in Fig. 5. The field of view is 20 × 20 µm^2. (**b**) Average depth profile obtained from 52 line profiles taken over the region limited by the two horizontal lines in (a)

ter. The different contours seen in that scanning electron micrograph delineate areas similar to those in Fig. 1 and with the same geometrical interpretation of the contours there. This assertion follows from Fig. 6(b) where an (averaged) atomic force depth scan proves that the contours are indeed elevations as they are depicted in the cross-sectional micrographs of Figs. 2(a), 3(a), and 4(a). In addition, the depth scan of Fig. 6(b) also establishes that the concentrically delineated areas are flat regions of increasing depths. Steps about 9, 9, and 22 nm deep can be identified in that ablation spot. Similar ablation steps are only hinted at in Fig. 1(b) because the laser beam used there was purposely laterally shaped to minimize intensity variations and the fluence was set just above threshold. Figure 5 is typical of spots that result when these precautions are not taken.

4 Discussion

The two questions raised initially can be answered positively. The $Ta_{42}Si_{13}N_{45}$ film can indeed be thinned fractionally in depth with femtosecond infrared laser pulses. And yes, the structure of the initially amorphous film remains amorphous after irradiation with a 200 fs laser pulse. All ternary alloys of the mictamict class share many common physical properties. It is hence consistent to surmise that these conclusions apply in a similar way to that class of materials as a whole when irradiated in a corresponding way.

It is difficult to compare the present results with those in the relevant literature. Cross-sectional transmission electron microscopy has been used sparingly to look sideways at the impact spot after femtosecond laser irradiation [5–15]. Most of these cases deal with single crystalline silicon as the target [7, 10, 11, 15]. Major issues addressed are the presence or absence of an amorphous layer of silicon in the ablation spot [8, 10, 11, 15], what strain and damage is induced in the silicon by a femtosecond pulse and how that depends on the fluence [7, 12]. Ablation spots of femtosecond lasers in alpha quartz [5], InP [9], 4H–SiC [13], GaP [14] and multi layers [6, 12] also have been analyzed in that fashion.

It is well known that succeeding irradiations of the same spot with the same laser pulse affect the target differently than the first pulse does. To be strict, only results derived from a single pulse of irradiation should therefore be compared with the present results. References [5] (α quartz), [11] (Si(100)), and [12] (multiple layers) report cross-sectional transmission electron micrographs for single femtosecond irradiations. Where the magnification would suffice to resolve 20 nm-sized pyramids as seen here in Figs. 2(b) or 4(a) and 4(b), none are visible (e.g., Fig. 9 in [11]). Even without restriction to a single irradiation pulse no indications of pyramids in the 10 or 20 nm range can be found. Randomly distributed sharp vertical features in the 10 to 20 nm range as seen in Figs. 2 and 4 have evidently never been observed before.

If a liquid state transiently arose during or after the femtosecond irradiation process of the $Ta_{42}Si_{13}N_{45}$ film, the results reported here offer no indication of its existence.

There are major obstacles on the way to interpreting the process of material removal observed here. Firstly, the results by themselves contain no direct information how the process proceeds in time. Furthermore, little is known about the physical properties of the $Ta_{42}Si_{13}N_{45}$ material itself other than random pieces of information: atomic composition (Ta:Si:N = 42:13:45), thickness (260 nm), approximate atomic density ($\sim 8.3 \times 10^{22}$ atoms/cm^3), that the material is structurally amorphous even under high resolution transmission electron microscopy. The surface of the film is extremely smooth (Rms = 0.17 nm) based on atomic force microscopy. The film is covered with a native oxide skin of unknown composition and of about 2 nm thickness. The film resists crystallization in vacuum under annealing for at least 30 min at 800°C. After 2 h at 1100°C the film decomposes. The constituents are hexagonal Ta_2N, tetragonal Ta_5Si_3, and hexagonal $Ta_{4.5}Si$ [4]. The melting points of these binary compounds at ambient pressure are quite high (e.g., 2960°C for Ta_2N, 2550°C for Ta_5Si_3). Amorphous silicon nitride

may be present as well. The film is mechanically brittle and hard. It has a greyish silvery lustre. At 800 nm wavelength and normal incidence the reflectivity is about 0.4 as measured by ellipsometry. The electrical resistivity is 740 μΩ cm at room temperature and has a nearly constant negative temperature coefficient of resistivity (-4 to 6×10^{-4}/K) from 3 to 500 K. A temperature dependence like this is quite uncommon and unlike those typical of semiconductors or metals. This piecemeal information on $Ta_{42}Si_{13}N_{45}$ limits the discussion to conceptual notions; quantitative evaluations are out of reach.

A hint to a plausible process involved in the ablation of the $Ta_{42}Si_{13}N_{45}$ film is contained in Figs. 6(a) and 6(b). In contrast to ablation spots observed in bulk materials where the depth profile is typically smooth and images that of the fluence profile of the laser beam, the spot depicted here consists of a sequence of level terraces of increasing depths and decreasing lateral extent. An image similar to that has been reported once before by Kononenko et al. [16]. The target there consisted of diamond-like amorphous carbon films 1 μm thick deposited on silicon substrates by two different methods. Similar results were observed for both film types over a wide range of parameters (pulses from 100 fs to 150 ns, wave lengths from 539 to 1078 nm). Up to 9 terraces were counted after the action of a single laser pulse.

That laser pulses can trigger shock waves moving inwards into the medium of the target and outwards into the ejected fluid is well known. Detailed experimental investigations of spallation in solid targets are nonetheless few [17–26]. Most of these have been executed on self-supported films of aluminium and copper and with the aim of verifying the accuracy of model simulations. In these experiments, spalls form at the "rear" side, i.e., at the side opposite to that where the laser beam impacts the film. This is so because a maximum of tensile strain forms near the open rear side of the film where the reflected compression wave—a rarefaction wave—and the rarefaction wave that follows the compression wave meet and overlap. When the film is deposited on a thick and heavy substrate, however, the initial compression wave and the rarefaction wave that follows it bounce back at the rear side again as compression and rarefaction waves. Spalling, if it occurs, then takes place at the open front side of the film.

Kononenko et al. [26] first encountered the phenomenon of "lift-off of material in the form of macroscopic sheets" when they irradiated diamond-like carbon films deposited on silicon wafers with 20 ns pulses of a KrF excimer laser (248 nm wave length). High local transient stresses were invoked as the cause, including the possibility of shock waves among other suggestions. Subsequent evidence [16] lead the group to conclude that the process is best attributed to the action of shock waves.

For multiple spallation to be possible, the energy of the shock wave must exceed by multiple times the energy necessary for a shock wave to traverse the film back and forth and then form and expel a scab after each round trip. In brittle materials, which the carbon and $Ta_{42}Si_{13}N_{45}$ films actually are, these processes are much less energy-intensive than in ductile materials such as aluminium and cupper. Where the fluence of the laser beam is highest, the waves are energetically strongest and can travel farthest. For a beam profile where the fluence peaks at the center, that means that the terraces are most numerous and deepest at the spot's center. When the light film rests on a massive substrate and the beam is broad in terms of the film thickness, the terraces will be flat. This is what Fig. 6 actually shows.

The shock wave model explains a number of observations reported here and also raises new questions. The model assumes that at least two distinct mechanisms exist for the removal of material by laser irradiation: (1) ablation, a process where the laser energy is directly transferred to the material that is subsequently relocated and/or ejected through various established or proposed mechanisms, and (2) spallation, where material is ejected by the action of shock waves. The latter is possible on the front side of the film (where the laser beam impacts the material) when the material is a thin film with small shock impedance [density x sound velocity] deposited on a thick substrate with large shock impedance. Shock effects are expected to be observable near the threshold fluence. At higher fluences, the direct transfer of energy to the material will prevail. That is clearly seen in Fig. 1 of [26] or in the present Fig. 3. The fluence used there exceeds that applied in Fig. 2. Signs in Fig. 3 can be interpreted as those of a thin layer that was removed by spallation, but where the major part of the missing material underwent some additional (probably thermal) type of transformation and ejection, as is revealed by the presence of bubble-like features in the remaining part of the film. The two mechanisms appear cumulated in this case. Why the spallation mechanism should lead to numerous nanoscale protrusions as revealed by the cross-sectional micrographs of Figs. 2 and 4 needs explaining. Have some of the mechanical properties of $Ta_{42}Si_{13}N_{45}$ been altered significantly by the direct coupling of the beam energy to the material by the time the shock wave has reached the surface after its first round trip? The shapes of the nanoprotrusions suggest a viscous flow. The evolution in time of the ablation mechanism versus that of the shock wave certainly will influence the range over which spallation dominates over ablation. Experimental conditions such as the configuration of the target, its material composition and the beam parameter are all expected to affect the final outcome.

The scenario depicted here is based on scant evidence. Additional experiments are clearly required to confirm or refute the proposed model. Additional tests should be made with thin films of stable and well characterized materials. $Ta_{42}Si_{13}N_{45}$ is an unusual solid that exists only in thin-film

form, is metastable and has no equation of state. Its particular nature may play a primary role on the particular outcome seen in Figs. 1 to 6. The amorphous diamond-like carbon films of [16] and [26] are also unusual and metastable. In all detailed experimental studies of spallation caused by short laser pulses that exist in the literature [16–26], back-spallation occurs only in just those two materials because they happen to be the only cases where the target happens to be configured in the way required for it [16, 26].

The tedious experimental nature of cross-sectional transmission electron microscopy precludes large systematic investigations of the present type. Choosing elemental combinations of a light, brittle, and stable film and a heavy substrate would open the door for quantitative comparisons with experimental results. Such an approach could test major aspects of the spallation model without transmission electron microscopy. It would also clarify which of the two proposed interpretations offered, if any, apply. In [16], spallation is claimed to arise because of the volume expansion in the near-surface region of the film combined with two shock waves emanating from it in opposite directions. Spalling should be observed only for materials like the examined diamond-like carbon films. In the present study, the shock wave and the rarefaction wave that follows it are believed to start at the film surface, bounce back from the rear interface and generate a spall at the surface as they are again reflected there. The mechanism could exist in most light thin films on heavy substrates and be observable under appropriate experimental conditions.

5 Final remark

The impact of heavy energetic ions into a solid target generates local hot spikes of target atoms whose evolution in time has been well studied. A primary ion in the range of 100 keV comes to rest in typically 10^{-13} s and initiates a collision cascade that ends in a dense ensemble of excited target atoms. It has been found that by 10^{-11} s local thermal equilibrium exists while the average particle energy is still in the eV range [27]. Although initially a laser pulse first transfers its energy to the target mainly via electrons while a swift ion mainly interacts directly with nuclei, the effect of very short laser pulses probably creates conditions not unlike those an energetic particle does. To what extent that similarity applies is unknown and is a subject worthy of investigation. Techniques similar to those used for ion-solid investigations would be one possible approach.

6 Conclusions

When a 260 nm-thick amorphous $Ta_{42}Si_{13}N_{45}$ film deposited on an oxidized silicon substrate is irradiated with a 200 fs laser pulse, it is possible to reduce the film's thickness by about 10% quite uniformly without inducing crystallization in the remaining film. The main mechanism responsible is attributed to spallation by a shock wave created by the laser pulse at the surface, as opposed to direct ablation of the material. The wave is presumably reflected back at the substrate interface and creates a scab as it returns to the surface. Uniformly distributed nanoscaled protrusions appear to be associated with that process. Another scenario has been proposed for a very similar experiment with a very similar result using diamond-like carbon films. Experiments are suggested how to clarify which of the two models, if any, applies. Whether insights gained from ion-solid investigations also apply to very short laser-solid interaction is mentioned as a worthwhile and challenging unsolved problem.

Acknowledgements We thank Dietmar Bertsch, NTB at Buchs (SG), who deposited the films and A. Dommann, CSEM at Neuchatel (NE), who executed the X-ray diffraction experiment. Special thanks go to André Koch for his input on shock waves. The resistivity of the $Ta_{42}Si_{13}N_{45}$ film from 3 to 500 K was measured at the I. Physikalisches Institut, University of Göttingen (Konrad Samwer) whom we gratefully acknowledge. We are also indebted to Willy Lüthy, IAP at University of Bern for taking scanning electron micrographs.

References

1. M. von Allmen, *Laser-Beam Interactions with Materials*, Springer Series in Materials Science, vol. 2 (Springer, Berlin, 1987)
2. D. Bauerle, *Laser Processing and Chemistry*, 3rd. edn. (Springer, Berlin, 2000)
3. M.-A. Nicolet, P.H. Giauque, Microelectron. Eng. **55**, 357 (2001)
4. E. Kolawa, P.J. Pokela, J.S. Reid, J.S. Chen, R.P. Ruiz, M.-A. Nicolet, IEEE Electron Device Lett. **12**(6), 321 (1991)
5. T. Gorelik, M. Will, S. Nolte, A. Tuennermann, U. Glatzel, Appl. Phys. A **76**, 309 (2003)
6. T. Höche, D. Ruthe, T. Petsch, Appl. Phys. A **79**, 961 (2004)
7. E. Coyne, J.P. Magee, P. Mannion, G.M. O'Conner, T.J. Glynn, Appl. Phys. A **81**, 371 (2005)
8. J. Jia, M. Li, C.V. Thompson, Appl. Phys. Lett. **84**, 3205 (2004)
9. A. Borowiec, M. Couillard, G.A. Botton, H.K. Haugen, Appl. Phys. A **79**, 1887 (2004)
10. Y. Izawa, Y. Izawa, Y. Setsuhara, M. Hashida, M. Fujita, R. Sasaki, H. Nagai, M. Yoshida, Appl. Phys. Lett. **90**, 044107 (2007)
11. T.H.R. Crawford, J. Yamanaka, G.A. Botton, H.K. Haugen, J. Appl. Phys. **103**, 053104 (2008)
12. T.H.R. Crawford, J. Yamanaka, E.M. Hsu, G.A. Botton, H.K. Haugen, Appl. Phys. A **91**, 473 (2008)
13. T. Okada, H. Kawahara, Y. Ishida, R. Kumai, T. Tomita, S. Matsuo, S. Hashimoto, M. Kawamoto, Y. Makita, M. Yamaguchi, Appl. Phys. A **92**, 665 (2008)
14. E.M. Hsu, T.H.R. Crawford, C. Maunders, G.A. Botton, H.K. Haugen, Appl. Phys. Lett. **92**, 221112 (2008)
15. M.S. Rogers, C.P. Grigorepoulos, A.M. Minor, S.S. Mao, Appl. Phys. Lett. **94**, 701111 (2009)
16. T.V. Kononenko, S.M. Pimenov, V.V. Kononeko, E.V. Zavedeev, V.I. Konov, G. Dumitru, V. Romano, Appl. Phys. A **79**, 534 (2004)
17. F. Cottet, M. Boustie, J. Appl. Phys. **66**(9), 4067 (1989)
18. S. Eliezer, I. Gilath, T. Bar-Noy, J. Appl. Phys. **87**(2), 715 (1990)
19. S. Eliezer, Y. Gazit, I. Gilath, J. Appl. Phys. **68**(1), 356 (1990)

20. V.E. Fortov, V.V. Kostin, S. Eliezer, J. Appl. Phys. **70**(8), 4524 (1991)
21. S. Courtier, T. de Rességuier, M. Hallouin, J.P. Romain, F. Bauer, J. Appl. Phys. **79**(12), 9338 (1996)
22. L. Tollier, R. Fabbro, E. Bartnicki, J. Appl. Phys. **83**, 1224 (1998)
23. L. Tollier, R. Fabbro, J. Appl. Phys. **83**, 1231 (1998)
24. W.H. Zhu, M. Yoshida, H. Tamura, K. Kondo, S. Tanimura, J. Mater. Sci. Lett. **20**, 961 (2001)
25. H. Tamura, T. Kohama, K. Kondo, M. Yoshida, J. Appl. Phys. **89**(6), 3520 (2001)
26. G. Dumitru, V. Romano, H. Weber, S. Pimenov, T. Kononenko, M. Sentis, J. Hermann, S. Bruneau, Appl. Surf. Sci. **222**, 226 (2005)
27. W.L. Johnson, Y.T. Cheng, M. van Rossum, M.-A. Nicolet, Nucl. Instrum. Methods B **7–8**, 657 (1985)